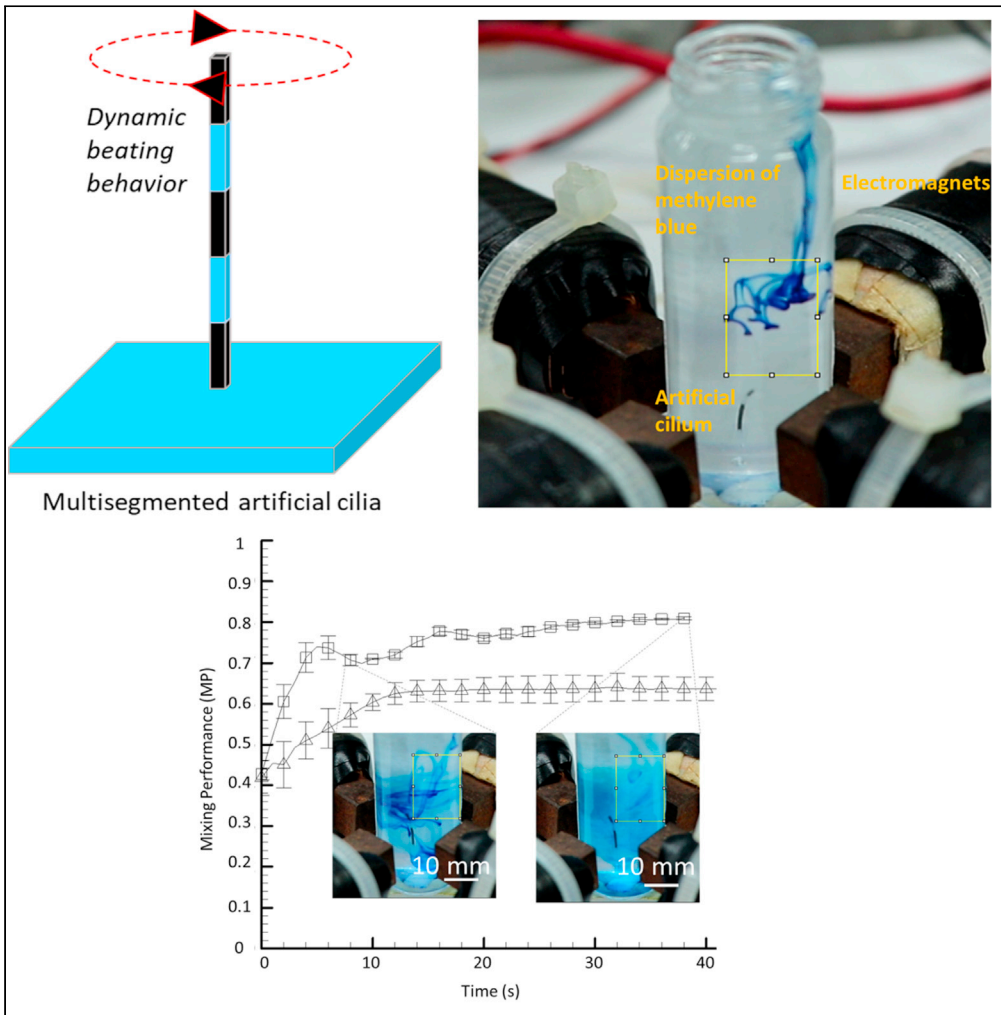


Article

Shape-programmable artificial cilia for microfluidics



Bivas Panigrahi,
Vignesh
Sahadevan, Chia-
Yuan Chen

chiayuac@mail.ncku.edu.tw

Highlights

Fabrication of artificial cilia was conducted through micromilling and casting methods.

The weighted index was correlated to the bending angles of artificial cilia.

Hydrodynamic analysis of artificial cilia was performed through the μ PIV analysis.

A significant improvement in mixing performance was achieved in few seconds.

Panigrahi et al., iScience 24, 103367
December 17, 2021 © 2021
The Authors.
<https://doi.org/10.1016/j.isci.2021.103367>



Article

Shape-programmable artificial cilia for microfluidics

Bivas Panigrahi,¹ Vignesh Sahadevan,² and Chia-Yuan Chen^{2,3,*}

SUMMARY

The artificial ciliary motion has been known not to be hydrodynamically optimal, limiting their associated applications in the microscale flow domain. One of the major hurdles of contemporary artificial cilia is its structural rigidity, which restricts their flexibility. To address this issue, this work proposed a shape-programmable artificial cilia design with distinctive polydimethylsiloxane (PDMS) and magnetic segments distributed throughout the structure, which provided precise control for time-spatial modulation of the whole artificial cilia structure under external magnetic actuation. For the fabrication of the proposed multi-segment artificial cilia, a facile microfabrication process with stepwise mold blocking followed by the PDMS and magnetic composite casting was adopted. The hydrodynamic analysis further elucidated that the proposed artificial cilia beating induced significant flow disturbance within the flow field, and the associated application was demonstrated through an efficient mixing operation.

INTRODUCTION

Bio-mimicking nature has long been an integral part of microfluidics research. The structure and functionality of natural sources are being mimicked with precision toward microfluidic environment control and flow manipulation (Chen et al., 2015; Fang et al., 2012; Hu et al., 2019; Li et al., 2017; Pekkan et al., 2016; Polachek et al., 2013). Such a notable example is artificial cilia, where natural cilia's design and locomotion have been mimicked with precision at the microscopic scale (Den Toonder et al., 2008, Shields et al., 2010; Chen et al., 2013; Huang et al., 2017). Considering the miniature size and high versatility in locomotion, these engineered structures were embedded within the microfluidic environment for flow manipulation. It can be noted that the motion of these microstructures can be controlled using magnetic, electrical, and pneumatic energy sources (Den Toonder and Onck, 2013). Using these external energy sources, the symmetric and asymmetric artificial cilia motion can be engineered toward achieving several microfluidic applications such as micromixing, micropropulsion, and even particle separation (Chen et al., 2014, 2016; Hanasoge et al., 2017; Zhang et al., 2020b). However, except few (Sareh et al., 2013), most artificial cilia reported to date are made up of a single rigid structure that can only be translated into two-dimensional (2D) spatial motion, limiting their microfluidic implementations. Hence, shape-programmable multi-segment artificial cilia are in the current demand, as it will provide a three-dimensional (3D) time-spatial flexibility to manipulate the in-depth flow within a microfluidic environment.

The shape-programmable matter has been the recent research interest, which allows the user to control their shape by the use of light (Huang et al., 2016), pneumatic (Martinez et al., 2012), chemicals (Wei et al., 2014), electric (Sareh et al., 2013), or magnetic fields (Lum et al., 2016). As these materials can be reshaped into the desired shape and form, their potential applications are quite lucrative in the field of miniaturized devices. Considering the fundamental principle of low Reynolds number flow, where the viscous force dominates the inertial force, to generate a definitive motion within the fluid flow environment, it is necessary to break the time-spatial asymmetry (Purcell, 1977). To create such kind of movement, micromachines made up of shape-programmable matter came into the picture. The utilization of these materials provided the micromachines an unprecedented mechanical function such as gripping, environmental sensing, flow manipulation. (Han et al., 2017; Xu et al., 2019). From all the aforementioned methods, magnetically actuated shape-programmable matter is considered promising as a complex shape-programmable microdevice can be created with facile fabrication methods, and their shape can be modulated with the least energy expenditure. To modulate the time-varying shapes of these devices, controlled external magnetic inputs in the forms of magnetic magnitude, as well as their spatial gradients, can be utilized.

¹Department of Refrigeration, Air Conditioning and Energy Engineering, National Cheng-Yi University of Technology, Taichung 411, Taiwan

²Department of Mechanical Engineering, National Cheng Kung University, No. 1 University Road, Tainan 701, Taiwan

³Lead contact

*Correspondence: chiayuac@mail.ncku.edu.tw
<https://doi.org/10.1016/j.isci.2021.103367>



A OVERALL FABRICATION PROCESS INVOLVING SUBFIGURES (I - V)

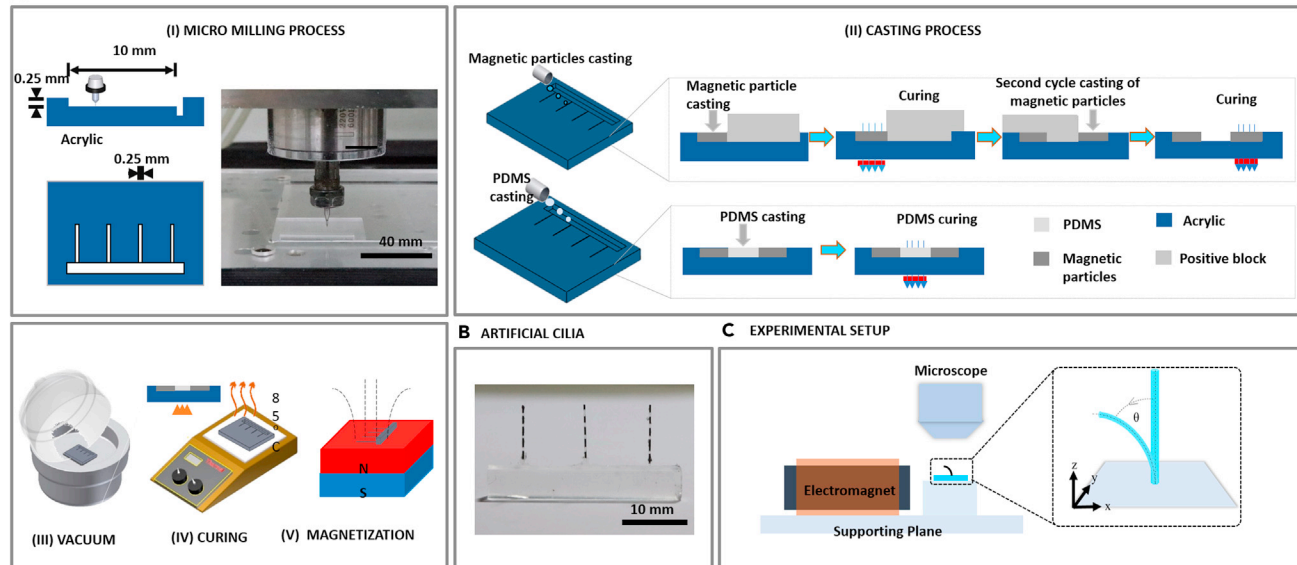


Figure 1. Schematic illustration of the proposed experimental setup

(A) A microfabrication process, which consists of a series of CNC micromilling processes followed by a PDMS casting method, was used to fabricate different types of artificial cilia.

(B) The real image of multi-segment artificial cilia with magnetic and PDMS segments.

(C) An in-house-developed electromagnetic actuation system that was used to test the performance of the artificial cilia with coordinate information provided.

Although subtle advances have been reported toward the design and fabrication of artificial cilia yet, most of these artificial cilia present to date are of single structure that can only mimic the motion of natural cilia, which is either conical or asymmetric pattern (Dong et al., 2020; Kim et al., 2017; Milana et al., 2019; Zhang et al., 2020a; Panigrahi et al., 2018; Lu et al., 2019; Gu et al., 2020). It has been realized that natural cilia motion is not hydrodynamically optimal (Guo et al., 2014); hence, imitating the natural cilia motion hinders the microfluidic performance. There have been significant research efforts put toward 3D printing of artificial cilia (Kamat et al., 2019; Azukizawa et al., 2018; Gu et al., 2020) in recent years. These artificial cilia with an improved structure were found effective toward flow manipulation, sensing, bending characteristics, and better magnetic control. However, with all the conventional methods, artificial cilia were fabricated with similar composition, and therefore, identical motions were generated corresponding to the homogeneous magnetic field. Although with the use of rotating magnets, the phase lag between two consecutive artificial cilia can be obtained, yet the artificial cilia will still exhibit the same beating behavior, limiting their hydrodynamic advantage in terms of flow manipulation. Considering that the artificial cilia's rigidity is one of the primary factors that hinder the development of engineered ciliary motion, this work initiates a shape-programmable multi-segment artificial cilia concept. In one of the relevant research studies by Sareh et al. (2013), biomimetic soft artificial cilia design was proposed where the natural motion of cilia was mimicked through a multi-segment ionic polymer-metal composite actuator (Sareh et al., 2013). Considering that Joule heating is a major issue associated with the electric field, the biomedical application of these cilia is partially restricted (Erickson et al., 2003). To address all these issues, this work proposed the design and the fabrication of a multi-segment artificial cilia structure that can be actuated through an external magnetic field. Considering that the proposed artificial cilia structure can be reshaped into various shapes through its multi-segment design uniqueness, the applications of these proposed artificial cilia within a microfluidic environment will be versatile.

RESULTS AND DISCUSSION

Bending characteristics

The design, fabrication, and actuation mechanism for multi-segmented artificial cilia is illustrated in the Figure 1 (see also Video S1). It was observed that corresponding to their exposure to the magnetic field, the individual cilia had illustrated diversely bending characteristics. A detailed description regarding the

estimation of the bending characteristic is provided in the [supplemental information](#). For Test case I, it was observed that upon the increase in magnetic segments ([Figure 2A](#)), the average bending angle of artificial cilia decreased significantly (left column of [Figure 2B](#)). For instance, when the magnetic segment was located at the tip of the artificial cilia (A1), the average bending angle of artificial cilia was accounted as $54.85 \pm 7.00^\circ$ ($n = 6$) compared with the value of $25.19 \pm 9.62^\circ$ ($n = 6$) when three magnetic segments were placed sequentially (A4). This highlights that an increase in the number of magnetic segments sequentially increased the structural rigidity of artificial cilium. For Test case II, it was further observed that irrespective of the position of the magnetic segments, the bending angle decreased with the increase in magnetic segments. However, even with the similar number of magnetic segments, the average bending angle changed, corresponding to the positioning of magnetic segments. For instance, artificial cilia with two magnetic segments distributed at different locations such as design D1 and D2, and the average bending angle was quantified as $31.13 \pm 11.12^\circ$ ($n = 6$) and $34 \pm 12.03^\circ$ ($n = 6$), respectively. It explains that when the magnetic segments were placed after 2 PDMS segments, rather than 1 PDMS segment, a net 10% increment in the bending angle can be achieved. This further confirmed that the distance between two consecutive magnetic segments might be playing a crucial role toward the structural rigidity of the artificial cilia. Furthermore, it was observed that when the magnetic segments were placed in the vicinity of the substrate, it significantly affected the bending ability of the artificial cilia. For instance, the bending angle for an artificial cilium D4 was found to be the lowest among all the designed artificial cilia.

It was observed that when the magnitude of WI of artificial cilia increased, the bending angle increased, and vice versa. For instance, for the artificial cilium A1 where the bending angle was found to be the maximum value of $54.85 \pm 7.00^\circ$, the WI was quantified as 75. Contrary to it, the WI for the artificial cilium D4 was quantified as minimum as 40, corresponding to its minimum bending angle of $11.31 \pm 7.24^\circ$. Considering the accuracy of WI to describe bending angle, it can be used to quantify the bending angle of the shape-programmable artificial cilia according to its design features.

Hydrodynamic analysis of artificial cilia bending

The flow field generated due to individual artificial cilia beating corresponding to time was further analyzed in the vicinity of the artificial cilia tip (highlighted as the focusing region of the inset [Figure 3A](#)). The instantaneous μ PIV velocity vectors out of the plane of the translational motion induced by the artificial cilia beating are illustrated in [Figure 3B](#). Instantaneous velocity contour maps are further provided to delineate the quantitative information ([Figure 3C](#)). As observed, a significant flow disturbance occurred in the vicinity of the artificial cilia tip, corresponding to the increase in time. In particular, the generated flow regime (green color) that is earlier noticed underneath the tip of artificial cilia (time frame of 0.016 s) displaced above the artificial cilia tip corresponding to the maximum time frame of 0.032 s. This further explains that the artificial cilia beating enhanced the flow disturbances, which is critical for flow propulsion as well as flow mixing within the microfluidic environment. On top of that, as the proposed multi-segment artificial cilia can be subjected to different bending behaviors corresponding to the same magnetic strength only by changing the position of the magnetic segments, it can be arranged to generate complex collective motion. For instance, if an individual cilium such as A1, A2, A3, and D2 is fabricated on a single substrate corresponding to a similar magnetic field, it will exhibit an average bending angle of $54.85^\circ \pm 7.00^\circ$, $48.48^\circ \pm 7.12^\circ$, $36.33^\circ \pm 12.78^\circ$, and $34.00^\circ \pm 12.03^\circ$, respectively. Considering the different bending characteristics of the four individually artificial cilia, it is possible that the consecutive cilia can exhibit a phase lag resulting in a collective wave which is the future direction of the current study.

Mixing operation

To elucidate the mixing performance (MP) achieved through the proposed artificial cilia actuation, flow visualization experiments were conducted with actuating artificial cilia. In this aspect, the methylene blue color was dispersed in the clear water, and its diffusion corresponding to time was noticed corresponding to the ciliary actuation. To quantify the dispersion of methylene blue, an area of $8.93 \times 12.45 \text{ mm}^2$ in the vicinity of an artificial ciliary location was selected. The MP was further quantified by implementing an algorithm that accounts for gray-level deviation of the captured images with respect to time, as illustrated underneath ([Chen et al., 2013](#)).

The magnitude of MP was quantified to be within a range from 0 to 1, where 0 illustrates no mixing and 1 illustrates complete mixing. As observed, when the artificial cilia were in a static position, the dispersion of methylene blue is minimal ([Video S2](#)). The mixing performances of the two modes (Mode I-Artificial cilia

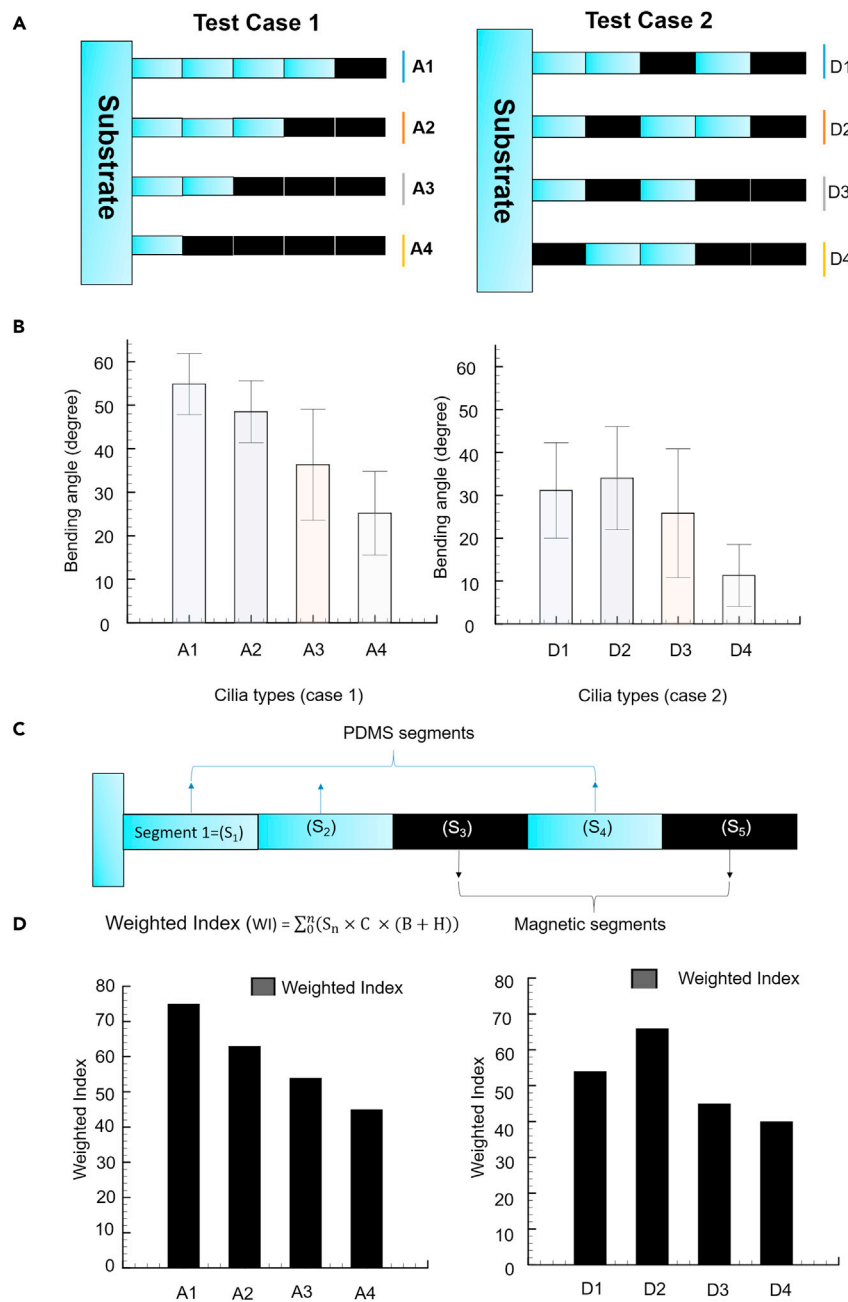


Figure 2. Bending angle corresponding to artificial cilia segmentation

(A) The schematic illustration of different artificial cilia test cases with varying magnetic segments distributed throughout the artificial cilia structure.

(B) The average bending angle of different artificial cilia corresponding to the magnetic field. The results are represented as mean \pm SD (n = 6).

(C) The weighted index (WI) is defined by accounting various factors such as segment positioning, bending factor, flexibility factor, continuity. It was observed the magnitude of WI is directly proportional to the bending angle of artificial cilia.

(D) The WI of the individual cilia with different compositions.

[5 Hz], Mode II- Static artificial cilia) over a time period of 40 s are presented in Figure 4. In Mode I, the artificial cilia were actuated in a conical manner rotating at a frequency of 5 Hz under the influence of the external magnetic field. It was observed that the diffusion of the blue ink with dispersing medium was quick

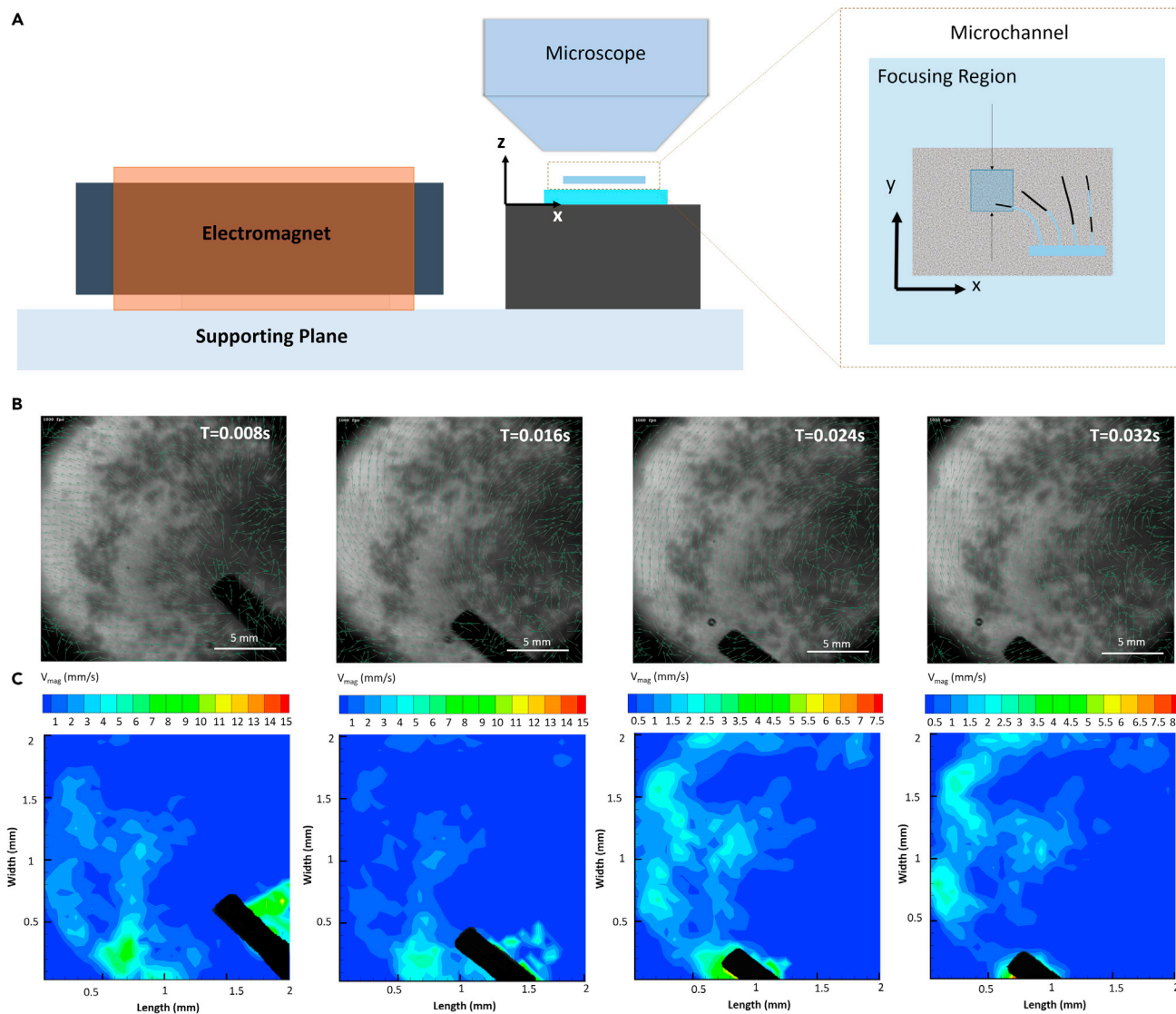


Figure 3. Imaging of flow visualization and experimental setup

(A) Experimental setup toward flow visualization experiment.

(B) Overlay images of tracing particles and instantaneous μ PIV velocity vector fields (green) corresponding to artificial cilia beating with respect to time.

(C) Time ensemble velocity contours in the vicinity of artificial cilia tip due to artificial cilia beating. The generated flow migrated from the bottom of the artificial cilia tip to the top of the artificial cilia with respect to time.

(the inset pictures of Figure 4). Upon quantification, a maximum MP was accounted as 0.81 ± 0.00 (mean \pm standard deviation [SD], $n = 3$) after the designated time period. Moreover, the lower magnitude in SD illustrates the uniform and stable mixing. Along with the conventional motion, these artificial cilia can additionally bend along z-direction to manipulate the corresponding flow, which can further advent diffusion within the in-depth microfluidic flow profile. This finding was compared with the control group (Mode II), where the artificial cilium was at static position. Upon quantification, it was observed that the maximum MP was as low as 0.64 ± 0.03 (mean \pm SD, $n = 3$). It was further observed that a uniform mixing for Mode I could be achieved in 6 s compared with 12 s of Mode II which suggested that Mode I is two times faster than that of Mode II. The percentage of increase in maximum mixing performance in Mode I was further noticed to 26.56%, compared with Mode II. The time required for the uniform mixing can be further decreased, and the maximum MP of the device can be further increased with an increase in the number of artificial cilia (Chen et al., 2016; Lu et al., 2019).

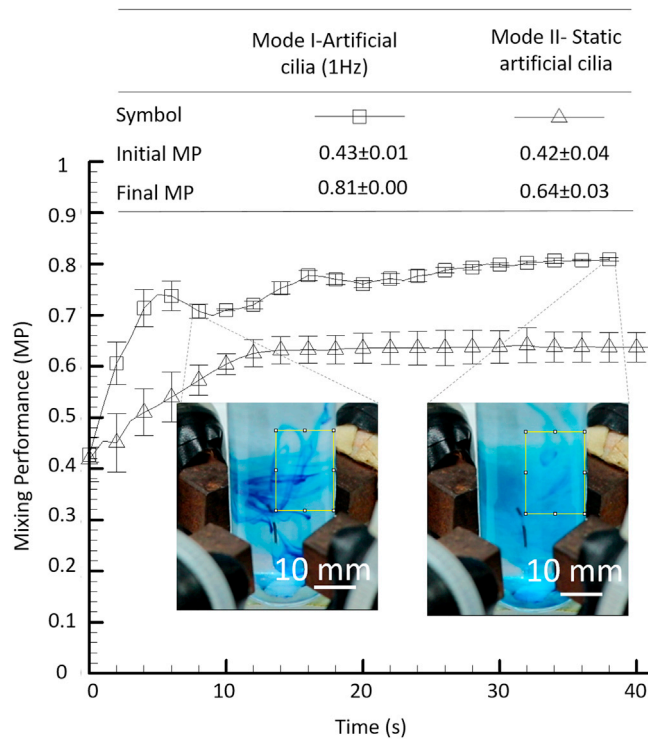


Figure 4. Time-dependent mixing performance (MP) with Mode I (artificial cilia actuation, beating frequency of 1Hz) and Mode II (static cilia)

The results illustrate the gradual dispersion of methylene blue within the medium corresponding to the time in the two cases. Results are represented as mean \pm SD ($n = 3$). The initial MP refers to the mixing performance quantified without artificial cilia actuation, and the final MP refers to the mixing performance quantified after a time period of 40 s.

Conclusions

This study proposed the shape-programmable artificial cilia with several magnetic as well as PDMS segments, which can be actuated through magnetic means. A facile and inexpensive microfabrication process was adopted for the fabrication of multi-segmented artificial cilia. Different designs of artificial cilia were tested to realize their bending characteristics corresponding to the external magnetic actuation. To correlate the bending phenomena of the artificial cilia according to the distribution of magnetic segments, a terminology WI was coined for the very first time in the literature. It was observed that the magnitude of WI is directly proportional to the bending phenomenon of artificial cilia. The results showed that through this new arrangement, each artificial cilium can perform distinct bending angles in the homogeneous magnetic fields, which demonstrated the future potentials of extending the artificial cilia toward a higher degree of motions collaboratively. The maximum mixing capacity of the artificial cilia was further accounted as high as 0.81 in 40 s of artificial cilia actuation. The applications of these magnetic shape-programmable cilia are widespread, ranging from micropropulsion, micromixing, to particle manipulation.

Limitations of the study

The present work was demonstrated through the reported test conditions, and further investigation for additionally practical applications may be necessary.

STAR★METHODS

Detailed methods are provided in the online version of this paper and include the following:

- [KEY RESOURCES TABLE](#)
- [RESOURCE AVAILABILITY](#)
 - Lead contact
 - Materials availability

- Data and code availability
- **METHOD DETAILS**
- Design and fabrication
- Magnetic actuation system
- Evaluation criteria for bending performance
- Flow visualization

SUPPLEMENTAL INFORMATION

Supplemental information can be found online at <https://doi.org/10.1016/j.isci.2021.103367>.

ACKNOWLEDGMENTS

This study was supported through the Ministry of Science and Technology of Taiwan under Contract No. MOST 108-2221-E-006-221-MY4 (to C.-Y.C.). This work would not be possible without the facility provided by the Center for Micro/Nano Science and Technology, National Cheng Kung University. This research was supported in part by Higher Education Sprout Project, the Ministry of Education to the Headquarters of University Advancement at National Cheng Kung University (NCKU).

AUTHOR CONTRIBUTIONS

Conceptualization, C.C.; investigation, B.P. and S.V; writing—original draft preparation, B.P.; writing—review and editing, B.P., S.V., and C.C.; supervision, C.C.; project administration, C.C.; funding acquisition, C.C.

DECLARATION OF INTERESTS

The authors declare no competing interests.

Received: February 18, 2021

Revised: June 13, 2021

Accepted: October 26, 2021

Published: December 17, 2021

REFERENCES

- Azukizawa, S., Shinoda, H., Tokumaru, K., and Tsumori, F. (2018). 3D printing system of magnetic anisotropy for artificial cilia. *J. Photopolym. Sci. Technol.* *31*, 139–144. <https://doi.org/10.2494/photopolymer.31.139>.
- Chen, C.-Y., Chen, C.-Y., Lin, C.-Y., and Hu, Y.-T. (2013). Magnetically actuated artificial cilia for optimum mixing performance in microfluidics. *Lab Chip* *13*, 2834–2839. <https://doi.org/10.1039/C3LC50407G>.
- Chen, C.-Y., Cheng, L.-Y., Hsu, C.-C., and Mani, K. (2015). Microscale flow propulsion through bioinspired and magnetically actuated artificial cilia. *Biomicrofluidics* *9*, 034105. <https://doi.org/10.1063/1.4921427>.
- Chen, C.-Y., Hsu, C.-C., Mani, K., and Panigrahi, B. (2016). Hydrodynamic influences of artificial cilia beating behaviors on micromixing. *Chem. Eng. Process. Process. Intensif.* *99*, 33–40. <https://doi.org/10.1016/j.cep.2015.10.023>.
- Chen, C.-Y., Lin, C.-Y., and Hu, Y.-T. (2014). Inducing 3Dvortical flow patterns with 2D asymmetric actuation of artificial cilia for high-performance active micromixing. *Exp. Fluids* *55*, 1765. <https://doi.org/10.1007/s00348-014-1765-x>.
- Den Toonder, J., Bos, F., Broer, D., Filippini, L., Gillies, M., De Goede, J., Mol, T., Reijme, M., Talen, W., and Wilderbeek, H. (2008). Artificial cilia for active micro-fluidic mixing. *Lab Chip* *8*, 533–541. <https://doi.org/10.1039/B717681C>.
- Den Toonder, J.M., and Onck, P.R. (2013). Microfluidic manipulation with artificial/bioinspired cilia. *Trends Biotechnol.* *31*, 85–91. <https://doi.org/10.1016/j.tibtech.2012.11.005>.
- Dong, X., Lum, G.Z., Hu, W., Zhang, R., Ren, Z., Onck, P.R., and Sitti, M. (2020). Bioinspired cilia arrays with programmable nonreciprocal motion and metachronal coordination. *Sci. Adv.* *6*, Eabc9323. <https://doi.org/10.1126/sciadv.abc9323>.
- Erickson, D., Sinton, D., and Li, D. (2003). Joule heating and heat transfer in poly (dimethylsiloxane) microfluidic systems. *Lab Chip* *3*, 141–149. <https://doi.org/10.1039/B306158B>.
- Fang, Y., Ye, Y., Shen, R., Zhu, P., Guo, R., Hu, Y., and Wu, L. (2012). Mixing enhancement by simple periodic geometric features in microchannels. *Chem. Eng. J.* *187*, 306–310. <https://doi.org/10.1016/j.cej.2012.01.130>.
- Gu, H., Boehler, Q., Cui, H., Secchi, E., Savorana, G., De Marco, C., Gervasoni, S., Peyron, Q., Huang, T.-Y., and Pane, S. (2020). Magnetic cilia carpets with programmable metachronal waves. *Nat. Commun.* *11*, 1–10. <https://doi.org/10.1038/s41467-020-16458-4>.
- Guo, H., Nawroth, J., Ding, Y., and Kanso, E. (2014). Cilia beating patterns are not hydrodynamically optimal. *Phys. Fluids* *26*, 091901. <https://doi.org/10.1063/1.4894855>.
- Han, K., Shields, C.W., Diwakar, N.M., Bharti, B., López, G.P., and Velez, O.D. (2017). Sequence-encoded colloidal origami and microbot assemblies from patchy magnetic cubes. *Sci. Adv.* *3*, E1701108. <https://doi.org/10.1126/sciadv.1701108>.
- Hanasoge, S., Ballard, M., Hesketh, P.J., and Alexeev, A. (2017). Asymmetric motion of magnetically actuated artificial cilia. *Lab Chip* *17*, 3138–3145. <https://doi.org/10.1039/C7LC00556C>.
- Hu, C., Chen, Y., Tan, M.J.A., Ren, K., and Wu, H. (2019). Microfluidic technologies for vasculature biomimicry. *Analyst* *144*, 4461–4471. <https://doi.org/10.1039/C9AN00421A>.
- Huang, H.-W., Sakar, M.S., Petruska, A.J., Pané, S., and Nelson, B.J. (2016). Soft micromachines with programmable motility and morphology. *Nat. Commun.* *7*, 1–10. <https://doi.org/10.1038/ncomms12263>.
- Huang, P.-Y., Panigrahi, B., Lu, C.-H., Huang, P.-F., and Chen, C.-Y. (2017). An artificial cilia-based micromixer towards the activation of zebrafish sperms. *Sens. Actuators B Chem.* *244*,

541–548. <https://doi.org/10.1016/j.snb.2016.12.113>.

Kamat, A.M., Pei, Y., and Kottapalli, A.G. (2019). Bioinspired cilia sensors with graphene sensing elements fabricated using 3D printing and casting. *Nanomaterials* 9, 954. <https://doi.org/10.3390/nano9070954>.

Kim, H.N., Jang, K.-J., Shin, J.-Y., Kang, D., Kim, S.M., Koh, I., Hong, Y., Jang, S., Kim, M.S., and Kim, B.-S. (2017). Artificial slanted nanocilia array as a mechanotransducer for controlling cell polarity. *ACS Nano* 11, 730–741. <https://doi.org/10.1021/acsnano.6b07134>.

Li, J., Wei, J., Liu, Y., Liu, B., Liu, T., Jiang, Y., Ding, L., and Liu, C. (2017). A microfluidic design to provide a stable and uniform in vitro microenvironment for cell culture inspired by the redundancy characteristic of leaf areoles. *Lab Chip* 17, 3921–3933. <https://doi.org/10.1039/C7LC00343A>.

Lu, C.-H., Tang, C.-H., Ghayal, N., Panigrahi, B., Chen, C.-Y., and Chen, C.-Y. (2019). On the improvement of visible-responsive photodegradation through artificial cilia. *Sens. Actuator A. Phys.* 285, 234–240. <https://doi.org/10.1016/j.sna.2018.10.045>.

Lum, G.Z., Ye, Z., Dong, X., Marvi, H., Erin, O., Hu, W., and Sitti, M. (2016). Shape-programmable magnetic soft matter. *Proc. Natl. Acad. Sci. U S A* 113, E6007–E6015. <https://doi.org/10.1073/pnas.1608193113>.

Martinez, R.V., Fish, C.R., Chen, X., and Whitesides, G.M. (2012). Elastomeric origami: programmable paper-elastomer composites as pneumatic actuators. *Adv. Funct. Mater.* 22, 1376–1384. <https://doi.org/10.1002/adfm.201102978>.

Milana, E., Gorissen, B., Peerlinck, S., De Volder, M., and Reynaerts, D. (2019). Artificial soft cilia with asymmetric beating patterns for biomimetic low-Reynolds-number fluid propulsion. *Adv. Funct. Mater.* 29, 1900462. <https://doi.org/10.1002/adfm.201900462>.

Panigrahi, B., Lu, C.-H., Ghayal, N., and Chen, C.-Y. (2018). Sperm activation through orbital and self-axis revolutions using an artificial cilia embedded serpentine microfluidic platform. *Sci. Rep.* 8, 4605. <https://doi.org/10.1038/s41598-018-22563-8>.

Pekkan, K., Chang, B., Uslu, F., Mani, K., Chen, C.-Y., and Holzman, R. (2016). Characterization of zebrafish larvae suction feeding flow using μ PIV and optical coherence tomography. *Exp. Fluids* 57, 112. <https://doi.org/10.1007/s00348-016-2197-6>.

Polacheck, W.J., Li, R., Uzel, S.G., and Kamm, R.D. (2013). Microfluidic platforms for mechanobiology. *Lab Chip* 13, 2252–2267. <https://doi.org/10.1039/C3LC41393D>.

Purcell, E.M. (1977). Life at low Reynolds number. *Am. J. Phys.* 45, 3–11.

Sareh, S., Rossiter, J., Conn, A., Drescher, K., and Goldstein, R.E. (2013). Swimming like algae: biomimetic soft artificial cilia. *J. R. Soc. Interf.* 10, 20120666. <https://doi.org/10.1098/rsif.2012.0666>.

Shields, A., Fiser, B., Evans, B., Falvo, M., Washburn, S., and Superfine, R. (2010). Biomimetic cilia arrays generate simultaneous pumping and mixing regimes. *Proc. Natl. Acad. Sci. U S A* 107, 15670–15675. <https://doi.org/10.1073/pnas.1005127107>.

Wei, Z., Jia, Z., Athas, J., Wang, C., Raghavan, S.R., Li, T., and Nie, Z. (2014). Hybrid hydrogel sheets that undergo pre-programmed shape transformations. *Soft Matter* 10, 8157–8162. <https://doi.org/10.1039/C4SM01299B>.

Xu, T., Zhang, J., Salehizadeh, M., Onaizah, O., and Diller, E. (2019). Millimeter-scale flexible robots with programmable three-dimensional magnetization and motions. *Sci. Robot.* 4. <https://doi.org/10.1126/scirobotics.aav4494>.

Zhang, S., Zhang, R., Wang, Y., Onck, P.R., and Den Toonder, J.M. (2020a). Controlled multidirectional particle transportation by magnetic artificial cilia. *ACS Nano* 14, 10313–10323. <https://doi.org/10.1021/acsnano.0c03801>.

Zhang, S., Zuo, P., Wang, Y., Onck, P., and Toonder, J.M.D. (2020b). Anti-biofouling and self-cleaning surfaces featured with magnetic artificial cilia. *ACS Appl. Mater. Inter.* 12, 27726–27736. <https://doi.org/10.1021/acami.0c05403>.

STAR★METHODS

KEY RESOURCES TABLE

REAGENT or RESOURCE	SOURCE	IDENTIFIER
Chemicals, peptides, and recombinant proteins		
PDMS	Dow Corning Corp., Midland, MI, USA	Sylgard 184
NdFeB particles	Magnequench, Singapore	MQP-15-7
Methylene blue	Liberty Stationery Corporation, Taiwan	Stamp Ink
Software and algorithms		
Dynamic Studio	Dantec Dynamics, Denmark	Dynamic Studio 2015a
ImageJ	National Institutes of Health (NIH)	https://imagej.nih.gov/ij/
LabVIEW	NI, Austin, Texas, United States	LabVIEW19.0f2 (64-bit)
Other		
Laboratory DC Power Supply	Instek, Taiwan	GPR-3510HD DC Power Supply
Data acquisition system	National Instruments, Austin, TX	NI-cDAQ-9174
High-speed camera	IDT, Tallahassee, FL, USA	NR4-S2
Fluorescent microscope	Olympus Corp., Japan	BX60

RESOURCE AVAILABILITY

Lead contact

Further information and requests should be directed to and will be fulfilled by the lead contact, Chia-Yuan Chen (chiayuac@mail.ncku.edu.tw).

Materials availability

The study did not generate new unique reagents.

Data and code availability

All data produced in this study are included in the published article and its [supplemental information](#), or are available from the lead contact upon request.

This paper does not report original code.

Any additional information required to re analyze the data reported in this paper is available from the lead contact upon request.

METHOD DETAILS

Design and fabrication

The dimensions of the artificial cilia are 10 mm in length (L), 0.25 mm in width (W), and 0.25 mm in thickness (T) as shown in [Figure 1B](#). The artificial cilia were designed to consist of five individual segments of PDMS and magnetic segments, each with 2 mm in length. To fabricate the multi-segment artificial cilia, a series of micromilling operations followed by the PDMS casting was employed. The fabrication process of artificial cilia is shown in [Figure 1A](#). Considering magnetic segments distributed throughout the length of cilia, a new microfabrication approach was adopted using CNC milling for the positional requirement of magnetic segments. To prepare for the magnetic segments, a uniform mixture of polydimethylsiloxane (PDMS, Sylgard 184, Dow Corning Corp., Midland, MI, USA) and magnetic particles (NdFeB, Neodymium Iron Boron Magnetic particles, MQP-15-7, Magnequench, Singapore) in a portion of 1:4 was poured into the mold for artificial cilia fabrication. Subsequently, the remaining portion of the mold was filled with PDMS solution, and the whole structure was degassed to remove any trapped particles. To obtain structural rigidity, the whole setup underwent a hotplate baking process at 85°C for an approximate period of 48 hr. The PDMS block with magnetic cilia was further peeled from the parent negative block and magnetized

according to the directional bending requirement through the use of a permanent magnet. Owing to the soft nature of PDMS structures connected with magnetic segments, it is easy to damage the artificial cilia while de-molding through the hand peeling process. To avoid this issue, the artificial cilia were manufactured with a higher length than the original size, and after peeling the artificial cilia from the acrylic mold, the artificial cilia were cut to the appropriate size. For instance, in the present work, artificial cilia were fabricated with 20 mm in length and cut to 10 mm length short after the peeling-off process. Small and appropriately sized tweezers were used to pull off the cilium from the acrylic mold to prevent the cilium from damage on the tip.

To elucidate the bending characteristics of the proposed multi-segment artificial cilia, experiments were conducted with the aid of a modified electromagnetic actuation system with a single electromagnet (Video S1). Two different artificial cilia setups denoted as Test case I and Test case II were used where the magnetic segments were distributed throughout the artificial cilia structure in a continuous or discrete manner to test the effectiveness of their arrangement. In particular, for Test case I, the magnetic segments were distributed sequentially, whereas, for Test case II, magnetic segments were discretely distributed throughout the ciliary structures.

Magnetic actuation system

To actuate artificial cilia, an in-house developed electromagnetic actuation setup was employed (Figure 1C). This actuation system was a combination of four individual electromagnets, a power supply (GPR-3510HD DC Power Supply, Instek, Taiwan), a data acquisition system (NI-cDAQ-9174, National Instruments, Austin, TX) with input modules, switching circuit, and an in-house developed GUI. In particular, four individual electromagnets were distributed equally in a horizontal plane, each with a separation angle of 90°. Each coil was made up of a rectangular iron bar (1.1 × 1.1 × 7.5 cm) wrapped with a single-strand 24-gauge magnetic coil for 800 turns. The setup was modified into a single electromagnet platform to test the bending phenomena of the proposed artificial cilia corresponding to the magnetic segment distribution. The power supply amplitude and duration were controlled through the GUI via a switching circuit. With an electric current supply of 4 A at 20 V to each of the electromagnetic actuators, the electromagnetic setup was able to generate a magnetic field up to 0.8 T.

Evaluation criteria for bending performance

To generalize the diverse bending phenomena and to explain the beating behavior corresponding to the distribution of the magnetic and PDMS segments (Figure S1), a term coined as weighted index (WI) was initiated for the very first time. The WI takes the consideration of various factors that affects the structural rigidity of cilia and was defined through the underneath equation.

$$WI = \sum_0^n (S_n \times C \times (B + H))$$

where S_n is defined as segment number which is valued as 1 to 5 counted from the base of artificial cilia (Figure 2C), B is the magnetic strength factor (considering the magnetic strength, it is indexed as 2 for magnetic segments whereas indexed as 1 for PDMS segments), H is the flexibility factor (it is indexed as 1 for magnetic segments whereas indexed as 2 for PDMS segments). C is the continuous factor which is indexed as 2 when either the PDMS or magnetic segments are positioned in a consecutive manner. Upon quantification, the magnitudes of WI were found to be directly correlated to the bending angles of artificial cilia (Figures 2B and 2D). The experimental bending characteristics of artificial cilia were further compared to analytical solid mechanics model and shared well agreement (Figure S2 and Table S1).

Flow visualization

To quantify the generated flow due to artificial cilia beating, micro-particle image velocimetry (μ PIV) analysis was used. To visualize the flow field, egg yolks were smashed, uniformly dispersed in the water, and introduced in a closed channel embedded with artificial cilia. It can be noted that the method was found to be biocompatible, relatively inexpensive, and accurate compared to traditional flow visualization with fluorescent particles and has been extensively used for μ PIV flow visualization. A high-speed camera (NR4-S2, IDT, Tallahassee, FL, USA) mounted on a fluorescent microscope (BX60, Olympus Corp., Japan) was used for flow visualization. Time-lapse images of the flow field due to artificial cilia beating were recorded at a frequency of 1000Hz. Commercially available PIV software (Dynamic Studio, Dantec Dynamics,

Denmark) was utilized for post-processing. An adaptive interrogation window size of 32×32 pixels was employed to quantify velocity vectors.

A divergent bending phenomenon was observed when the magnetic segments were distributed throughout the ciliary structures. To further evaluate the performance of artificial cilia toward flow mixing operation, experiments were conducted (Video S2). In this aspect, artificial cilia were fixed within a glass tube meanwhile immersed within water. Methylene blue (100% by weight) was introduced into the glass tube using a micropipette, and artificial cilium was actuated circularly using an electromagnetic actuation system. Time-lapse images were recorded using the aforementioned imaging setup utilized for μ PIV analysis. A series of image processing techniques were implemented through free and open-source software ImageJ. In particular, the mixing performance was evaluated in the vicinity of the artificial cilia tip by quantifying the intensity difference in the consecutive images. Mixing performance was evaluated by measuring the gray level difference of the recorded images during mixing (Equation 1). To precisely observe the mixing performance under the influence of the magnetically actuated cilia, it was compared with the control group where is the participation of the cilium is absent.

$$\text{Mixing performance (MP)} = 1 - \frac{1}{\bar{m}} \sqrt{\frac{\sum_{i=1}^n (m_i - \bar{m})^2}{n}} \quad (\text{Equation 1})$$

where m_i is an intensity value of each pixel in the selected region of interest on the imaging plane, and \bar{m} is the arithmetic average of m_i . The mixing index of 0 refers to no mixing, whereas 1 refers to the complete mixing.